Hvězdná noc, 1889

Struktura a kinematika galaxií (F7567)
Dynamika a vývoj galaxií (F8567)

Bruno Jungwiert

Astronomický ústav AV ČR, v.v.i.

bruno.jungwiert@ig.cas.cz

F7567/F8567, PřF MU Brno, 2016/2017

Program přednášky:

I. Klasifikace galaxií
Hmotnostní, prostorové a časové škály

II. Složky galaxií: bulge, disk, halo, spirální ramena, příčky, hvězdokupy
Hvězdy, plyn, temná hmota

III. Profily svítivosti
Luminozitní funkce

IV. Gravitační potenciál
Dvojice potenciál-hustota

V. Dráhy v galaxiích

VI. Rovnováha bezsrážkových systémů
Rozdělovací funkce
Boltzmannova rovnice
Jeansovy rovnice

VII. Gravitační nestabilita
Teorie spirálních hustotních vln
Příčky, dvojpříčky

VIII. Interakce galaxií
Slapové síly, dynamický tlak
Dynamické tření
Galaktický kanibalismus

IX. N-částicové simulace

X. Vznik hvězd, aktivní galaktická jádra, koevoluce galaxií a centrálních černých děr

IX. Vznik galaxií
Expanze vesmíru

KAPITOLA I

I.1. Základní klasifikace galaxií
(Hubble, de Vaucouleurs)

I.2. Bulge, příčky, dvojpříčky, prstence, nukleární spirály

I.3. Radiální profily plošné jasnosti
(Hubble-Reynolds, modifikovaný Hubbleův profil, de Vaucouleurs, Sérsic, Freeman)

Obrázky a vzorce, u nichž není uveden zdroj, jsou převzaty z učebnice Galactic Dynamic (Binney & Tremaine 1987)

Leviathan Telescope (1,8m-mirror), Parsonstown, Ireland (1845):

spiral nebulae discovered by lord Rosse

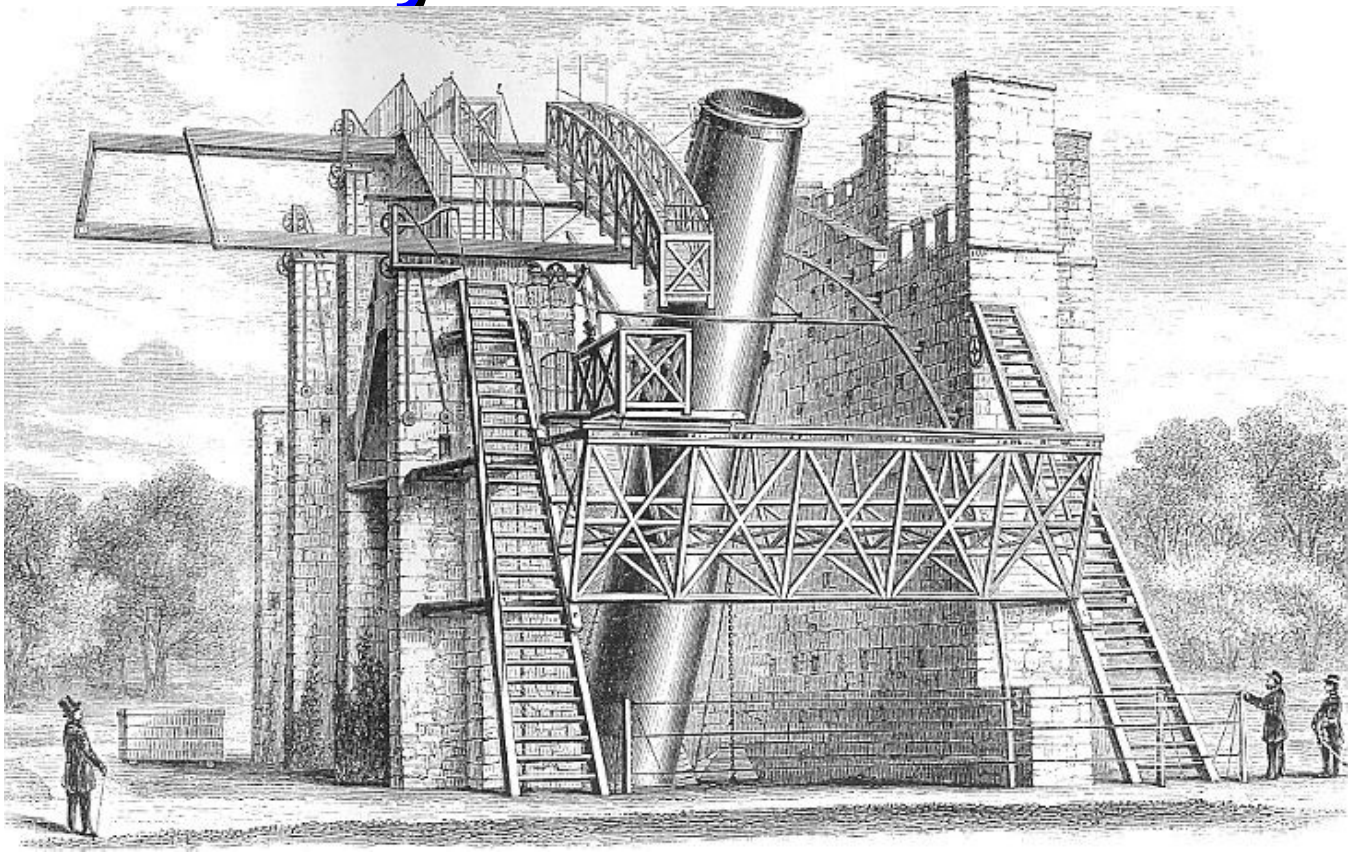

source: Telescopes.stardate.org, webpage: stardate-Levia

Lord Rosse's drawings of M51, his "Question Mark" "Spiral Nebula"

left:
Rosse's drawing (1846) - the first “spiral nebula”
right:
a modern photo of the same galaxy (called M51 or “Whirlpool Galaxy”
(see also its *HST* image – 2 slides back)

http://messier.seds.org/more/m051_rosse.html

Lord Rosse's drawing of M99

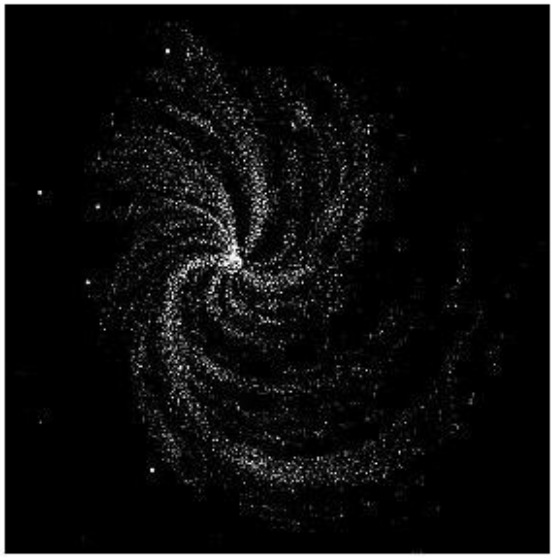

William Parsons (Lord Rosse):

M51 (1846)

M99 (1848)

But ***the true nature of spiral nebulae***, now called spiral galaxies (large systems composed of stars and lying outside our own Galaxy, as independent stellar islands), ***remains unknown until*** *1924*.

http://messier.seds.org/more/m099_rosse.html

1924, Galaxies and the „Great Debate”

1925, The Hubble Sequence (The Hubble classification of galaxies)
Edwin P. Hubble, Mt. Wilson, California

elliptical galaxies (E), lenticular galaxies (S0),
normal spirals (S), barred spirals (SB),
irregular galaxies (I)

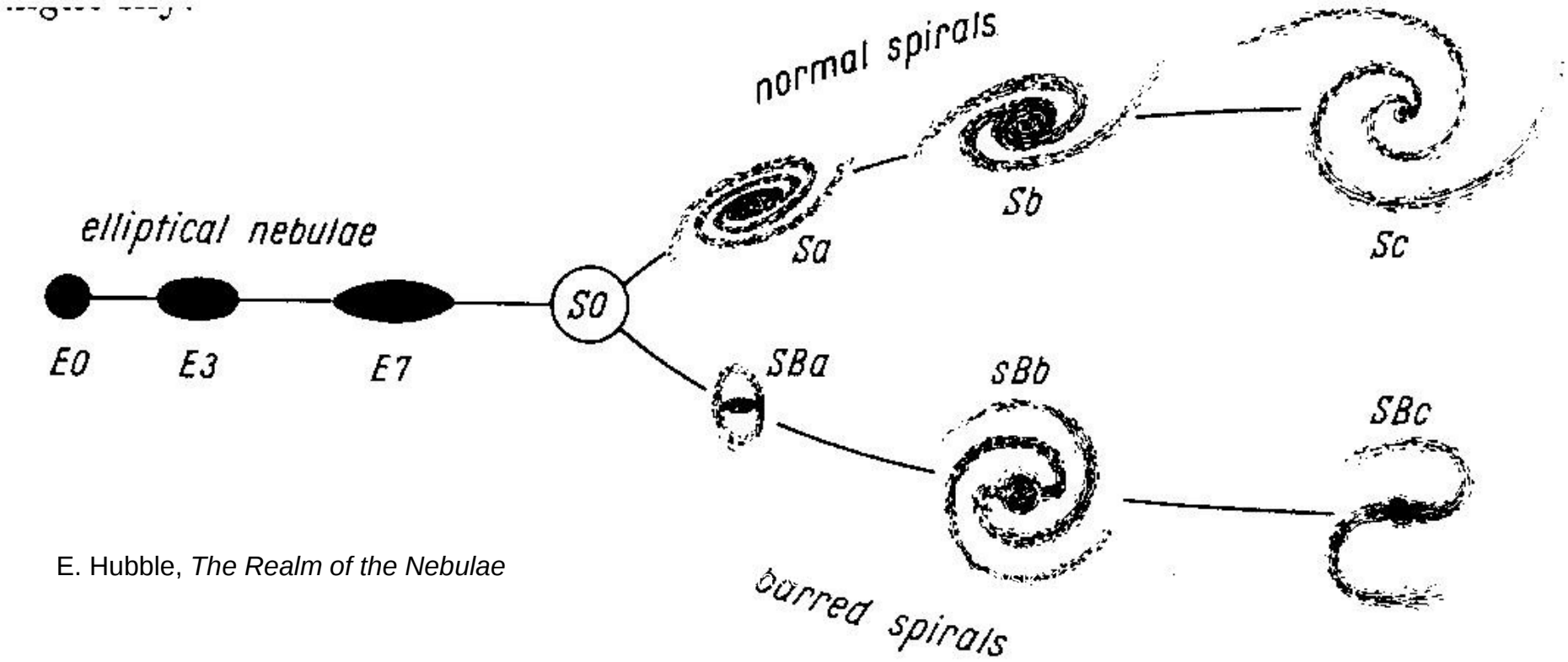

E. Hubble, *The Realm of the Nebulae*

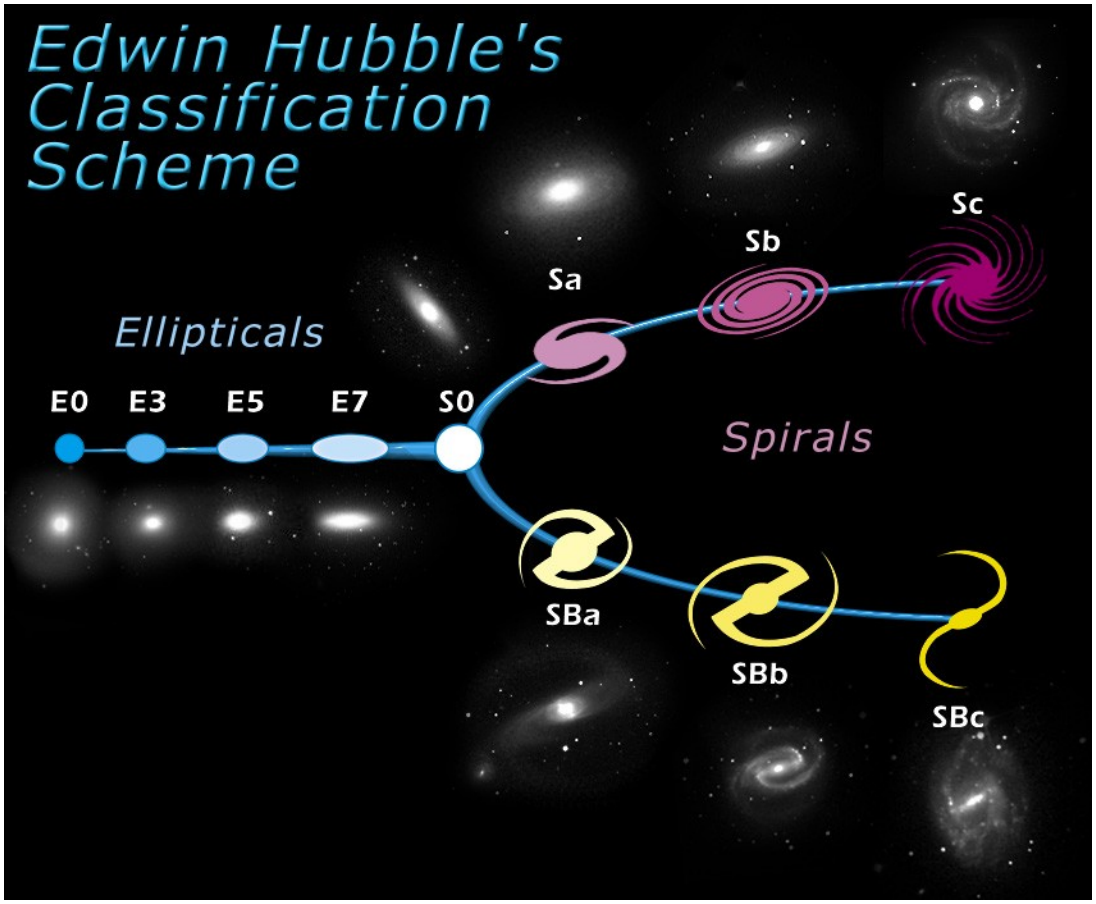

Edwin P. Hubble (1889 - 1953)

Classification of galaxies (1925)
Measuring speeds of galaxies → expansion of the Universe discovered (1929)

Images: https://en.wikipedia.org/wiki/File:HubbleTuningFork.jpg, https://en.wikipedia.org/wiki/File:Edwin-hubble.jpg

Hooker telescope (100-inch mirror)

Mt. Wilson, California

Fundamental discoveries:

- nature of spiral nebulae: **galaxies**
- speeds of galaxies: **expansion of the Universe**

The Hubble tuning fork (1925, Mt. Wilson)

Elliptical (E), lenticular (S0), normal spiral (S), barred spiral (SB) and irregular galaxies (I)

E sub-types: E0 – E7, n = 10(1 – b/a)

S and SB sub-types: Sa, Sb, Sc and SBa, SBb, SBc

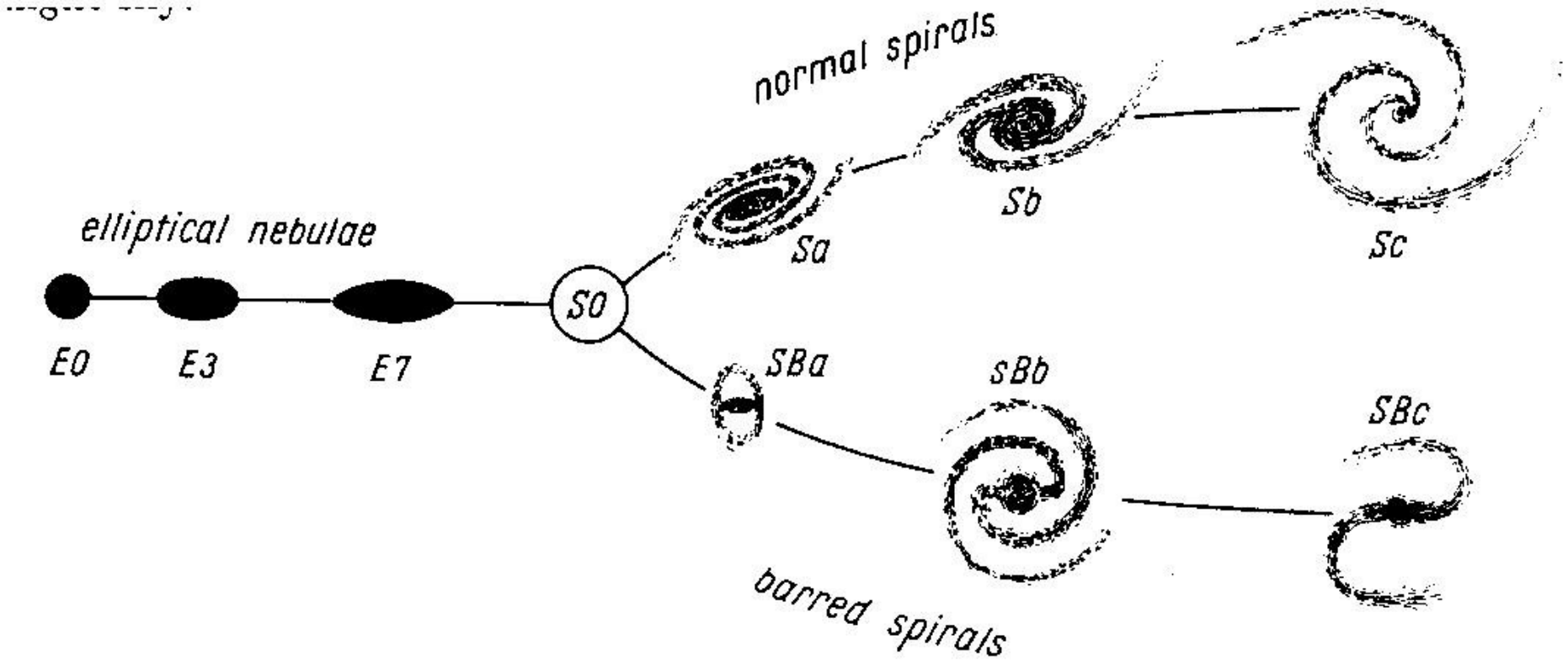

from: G. de Vaucouleurs, Classification and Morphology of External Galaxies, Handbuch der Physik, 1959, Vol. 53, pp. 275-310

http://nedwww.ipac.caltech.edu/level5/Dev/frames.html

Spiral Galaxy Messier 83
(FORS / VLT)

ESO PR Photo 24b/05 (August 10, 2005) © ESO

Spiral Galaxy NGC 4565
(FORS / VLT)

ESO PR Photo 24a/05 (August 10, 2005) © ESO

elliptical galaxies,
normal spiral galaxies,
barred spiral galaxies

face-on views
edge-views

The Sombrero Galaxy (VLT ANTU + FORS1)

ESO PR Photo 07a/00 (22 February 2000) © European Southern Observatory

The de Vaucouleurs classification (1959, 1964)

- classes E, S0, S, Im
- families A, AB, B
- varieties s, rs, r

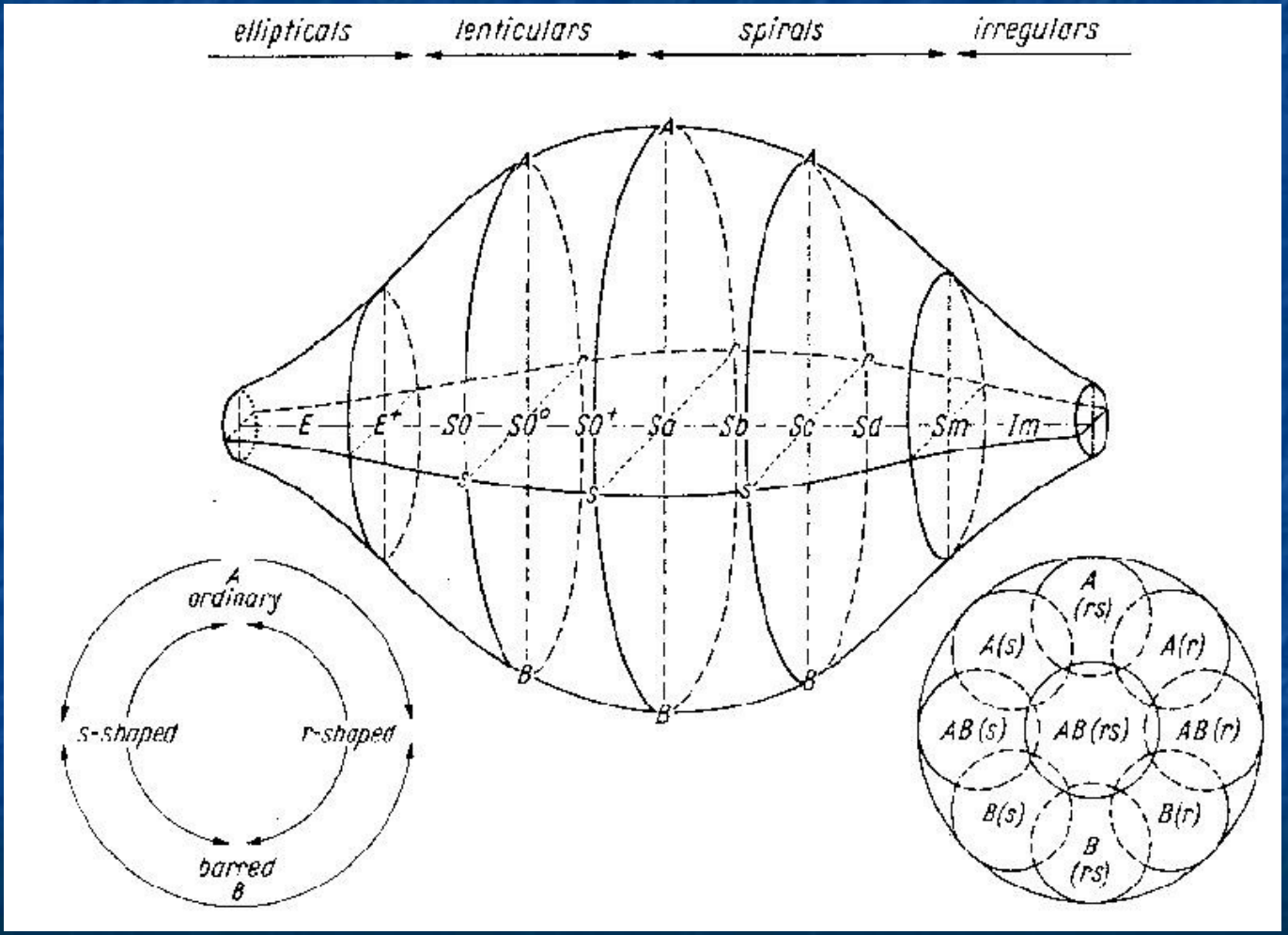

from: G. de Vaucouleurs, Classification and Morphology of External Galaxies, Handbuch der Physik, 1959, Vol. 53, pp. 275-310

http://nedwww.ipac.caltech.edu/level5/Dev/frames.html

De Vaucouleurs (1959)

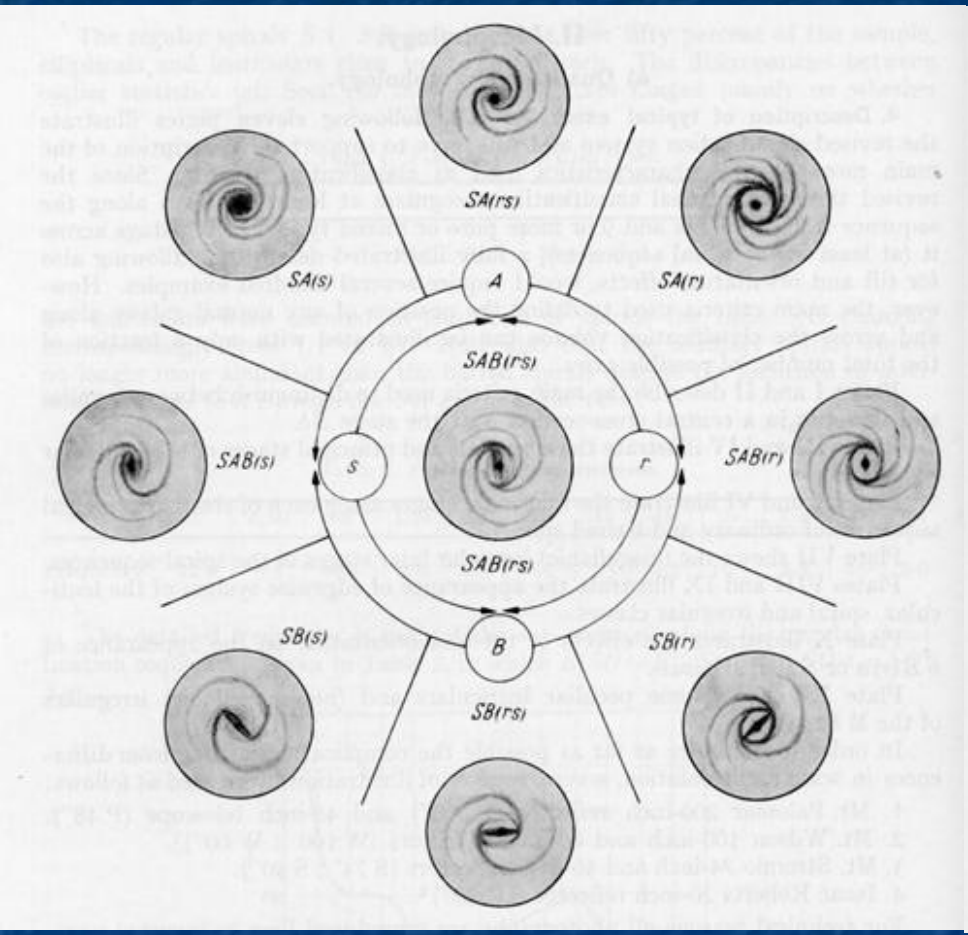

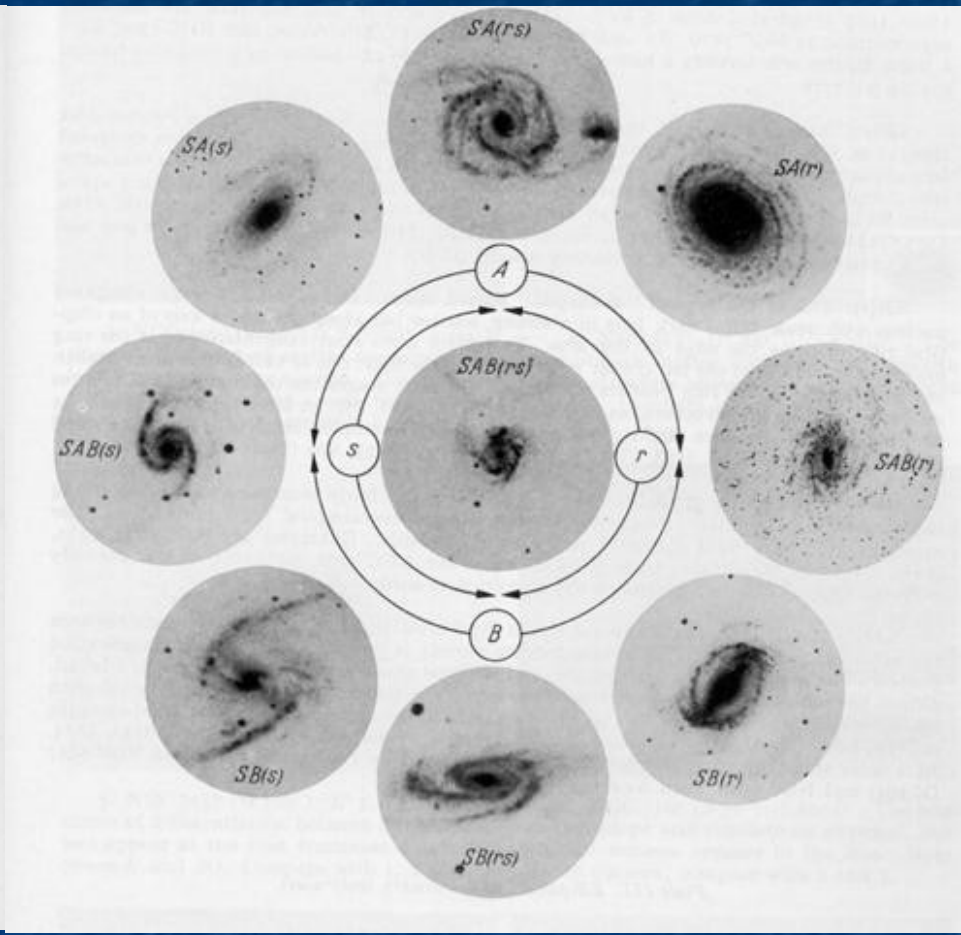

from: G. de Vaucouleurs, Classification and Morphology of External Galaxies, Handbuch der Physik, 1959, Vol. 53, pp. 275-310

http://nedwww.ipac.caltech.edu/level5/Dev/frames.html

Bulges

M 104 SA(s)a
NGC 4565 SA(s)b?

B/D – bulge-to-disk ratio
B/T = B/(B+D) – bulge-to-total luminosity ratio

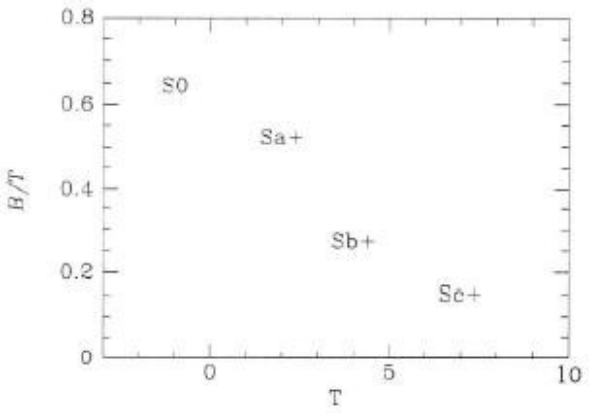

(zdroj: Binney & Merrifield, Galactic Astronomy, kapitola IV)

Figure 4.51 The later the Hubble stage T of a disk galaxy, the smaller is its bulge fraction B/T. The plotted values are means. Individual values scatter significant about these means. [From data published in Kent (1985)]

SA(s)a

SA(s)b

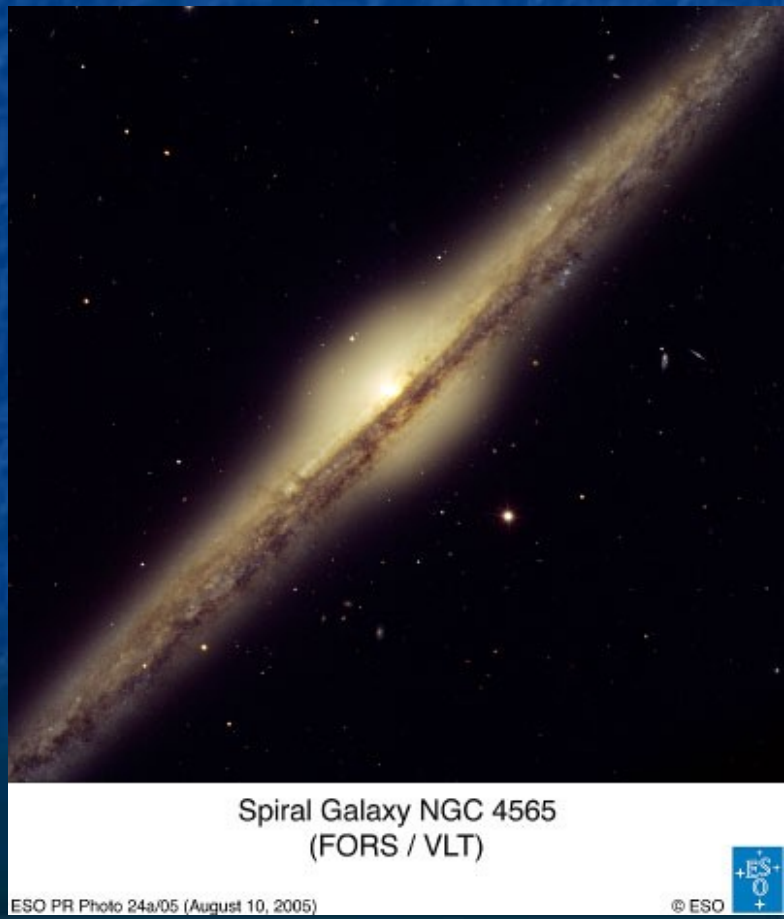

Bars (příčky)

> 2/3 diskových galaxií mají příčku viditelnou v optickém oboru

typ SA: galaxie bez příčky ~1/3
typ SAB: galaxie se ,,slabou" příčkou ~1/3
typ SB: galaxie se ,,silnou" příčkou ~1/3

v blízké infračervené oblasti je frekvence příček > 80%

SAB(s)c

Spiral Galaxy Messier 83
(FORS / VLT)

ESO PR Photo 24b/05 (August 10, 2005) © ESO

SAB(rs)cd

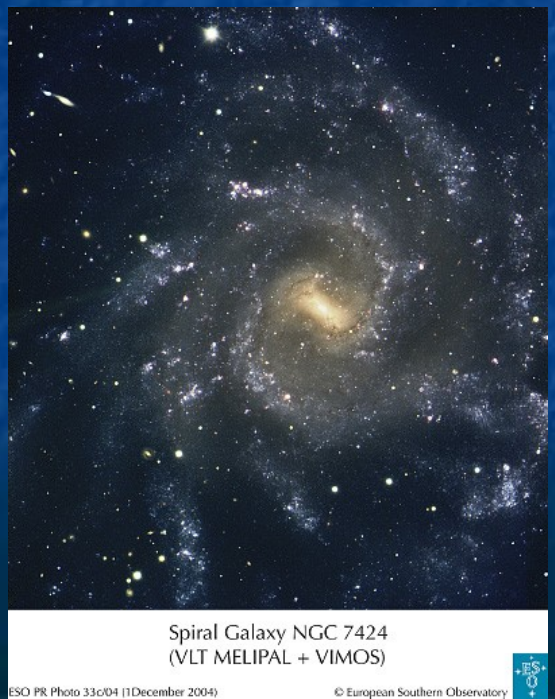

Spiral Galaxy NGC 7424
(VLT MELIPAL + VIMOS)

ESO PR Photo 33c/04 (1December 2004) © European Southern Observatory

SB(r'l)b

Spiral Galaxy NGC 1097
(VLT MELIPAL + VIMOS)

ESO PR Photo 35d/04 (22 December 2004) © European Southern Observatory

Dvojpříčky (double bars, bars-in-bars)
Nukleární příčky (nuclear bars, baby bars)

Double bar in NGC 1433 (R'$_1$ SB(rs)ab)

(B band, Buta & Combes 1996)

(H band, JCA, 1997)

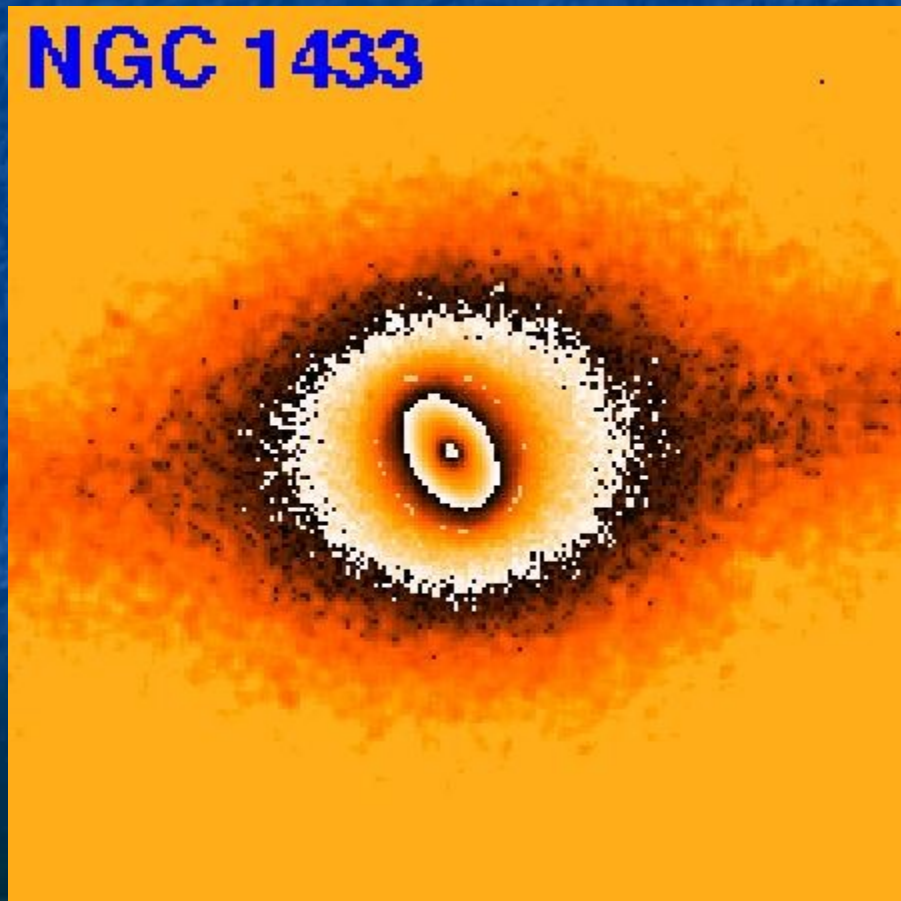

Prstence (rings) a pseudo-prstence (pseudo-rings) v diskových galaxiích

označení:

	prstence	pseudo-prstence
- vnější (outer):	R, R_1, R_2	R', R'_1, R'_2
- vnitřní (inner):	r	rs (nebo r')
- nukleární:	nr	nr'

Příklady vnějších a vnitřních prstenců

NGC 7020 (Buta & Combes 1996)
(R)SA(r)0$^+$

(R'$_1$)SB(r)ab (Sy)

(R'$_2$)SAB(r)b

Nukleární prstenec v NGC 1097

SB(r'l,nr)b

Spiral Galaxy NGC 1097
(VLT MELIPAL + VIMOS)

ESO PR Photo 35d/04 (22 December 2004) © European Southern Observatory

The Centre of the Active Galaxy NGC 1097
(NACO/VLT)

ESO PR Photo 33a/05 (October 17, 2005) © ESO

Nukleární spirály

NGC 1365, SB(s)b

optical image

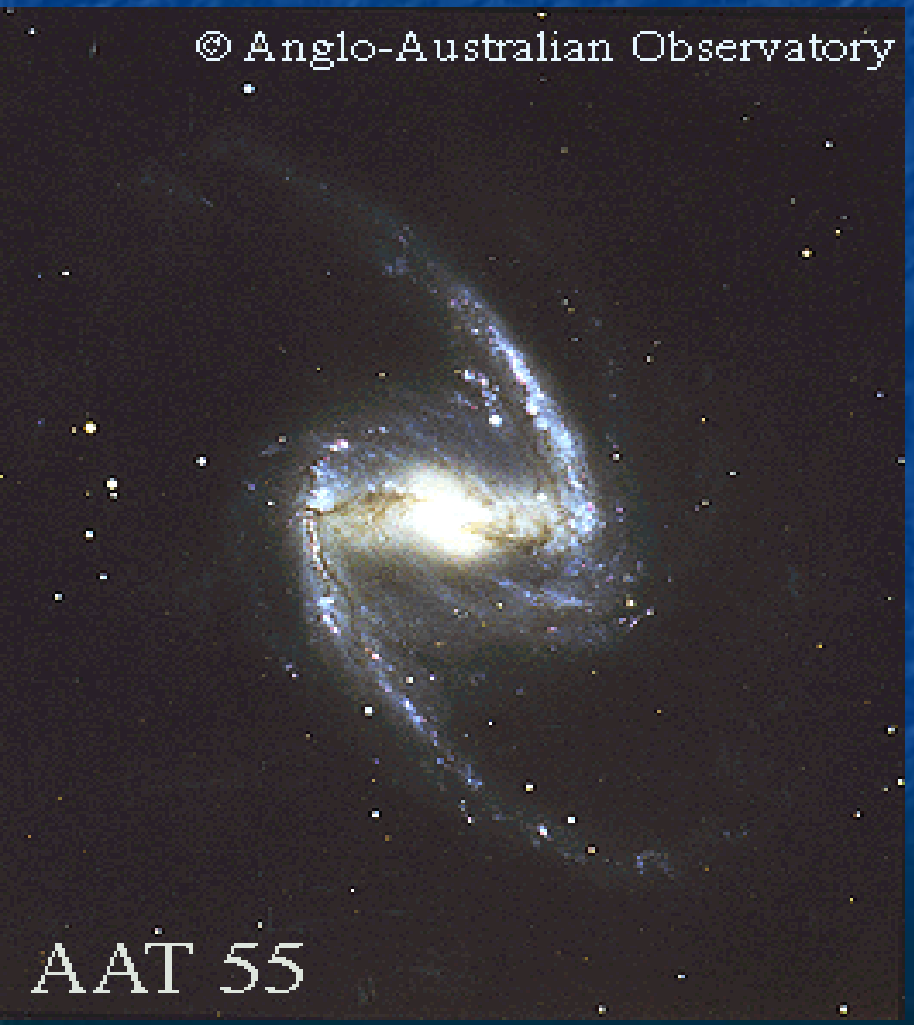

near-IR image (H-band)

(different scale; from JCA, 1997)

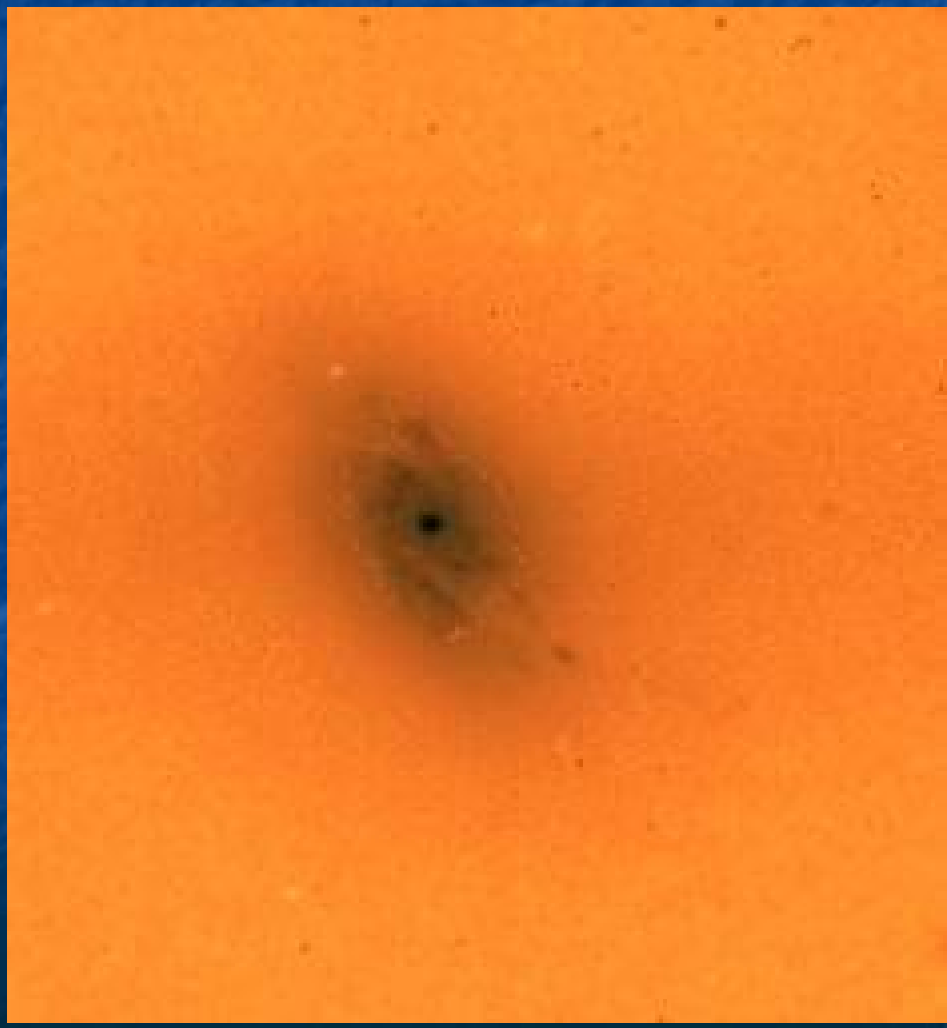

Frekvence typů (tříd) a podtypů galaxií:

Hubble (1926)

Type:	E	Sa/SBa	Sb/SBb	Sc/SBc	I
	17%	19%	25%	36%	2.5%

Shapley and Ames (1926) – Coma-Virgo region

E	S	I
47%	48%	5%

-> environmental dependence

de Vaucouleurs (1959)

Frequency of revised types:

Type:	E	S0	SA	SB	I	Pec
	23%	21%	24%	26%	3.4%	1.5%

Frequency (%) of subdivisions:

Type:	E	E/S0	S0	S0/a	Sa	Sab	Sb	Sbc	Sc	Scd	Sd	Sm
	22	9.5	10.5	9	4.5	6.5	7.5	7.5	10.5	8.5	2.0	2.0%

Grand-design spirals vs. flocculent (stochastic) spirals

M 81 SA(s)ab

NGC 2841 SA(r)b

Credit: M81: Stefan Seip/Adam Block/NOAO/AURA/NSF, http://www.noao.edu/outreach/aop/observers/m81.html
NGC 2841: Peter Kukol/Adam Block/NOAO/AURA/NSF, http://www.noao.edu/outreach/aop/observers/n2841.html

M 101 SAB(rs)cd

NGC 7217 SAab

NGC 488 SA(r)b

Credit: NGC 7217 and M 101: Adam Block/NOAO/AURA/NSF
NGC 488: Tony Kriz/Adam Block/NOAO/AURA/NSF

Surface brightness profiles (profily plošné jasnosti)

1) Elliptical galaxies

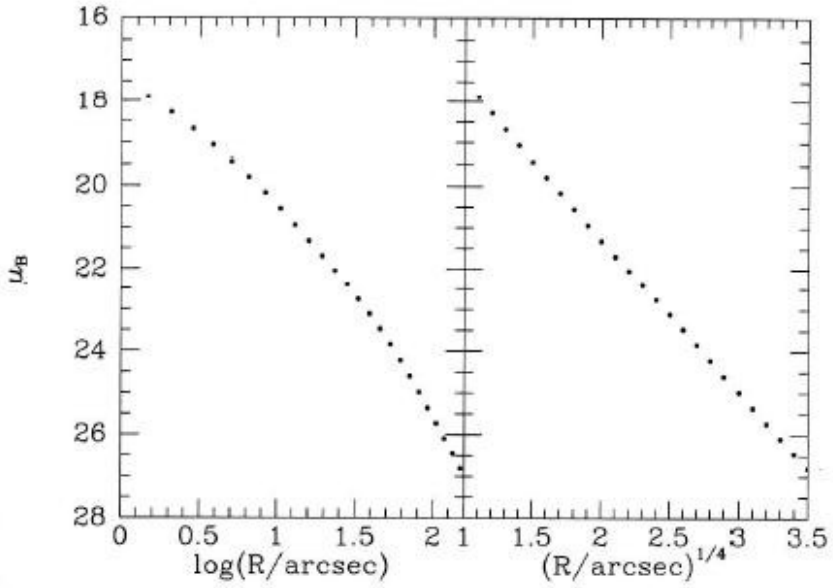

Figure 4.25 The major-axis brightness profile of NGC 1700 plotted against (a) $\log r$ and (b) $R^{1/4}$. [From data published in Capaccioli, Piotto & Rampazzo (1988)]

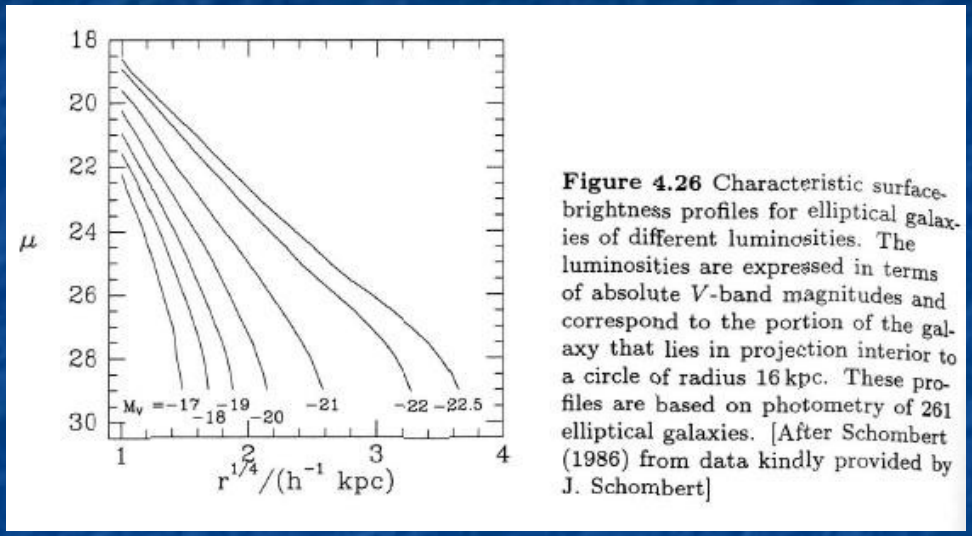

Figure 4.26 Characteristic surface-brightness profiles for elliptical galaxies of different luminosities. The luminosities are expressed in terms of absolute V-band magnitudes and correspond to the portion of the galaxy that lies in projection interior to a circle of radius 16 kpc. These profiles are based on photometry of 261 elliptical galaxies. [After Schombert (1986) from data kindly provided by J. Schombert]

de Vaucouleurs profile (1948), $R^{1/4}$-law

$$I(R) = I_e 10^{\{-3.33[(R/R_e)^{1/4}-1]\}}$$
$$= I_e \exp\{-7.67[(R/R_e)^{1/4}-1]\}$$

$$2\int_0^{R_e} \mathrm{d}R\, I(R) 2\pi R = \int_0^{\infty} \mathrm{d}R\, I(R) 2\pi R$$
$$= \frac{8!\,\exp(7.67)}{(7.67)^8}(\pi R_e^2 I_e) = 7.22\pi R_e^2 I_e$$

Zdroj: Binney & Merrifield, Galactic Astronomy

Diffuse dwarf elliptical galaxies: exponential profiles

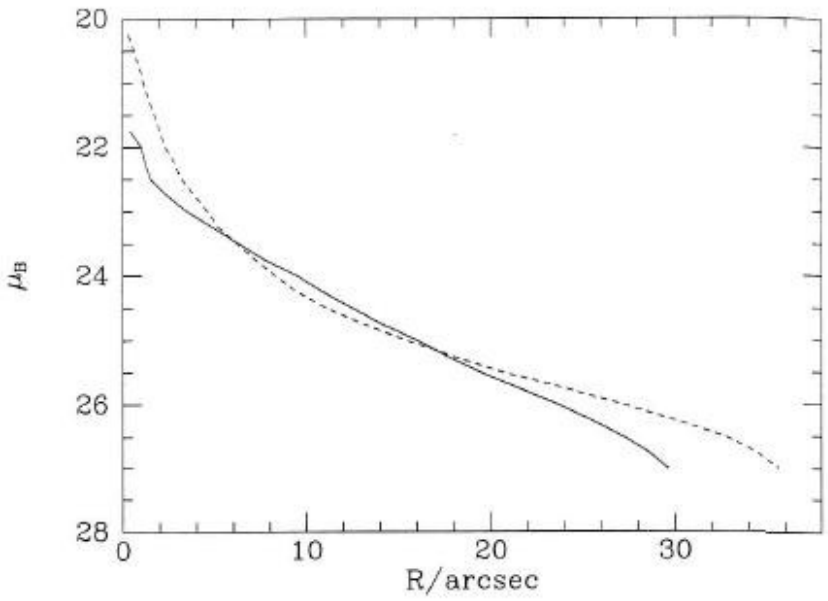

Figure 4.30 The full curve shows the surface-brightness profile of a typical dE galaxy in the Virgo cluster from the photographic photometry of Ichikawa, Wakamatsu & Okamura (1986). Note that the profile is nearly straight in this log-linear plot because it is well fitted by the exponential law (4.20). The dashed curve shows the surface brightness profile of another galaxy from the same study. This galaxy approximately obeys the $R^{1/4}$ and is thought to be a background giant elliptical galaxy.

Zdroj: Binney & Merrifield, Galactic Astronomy

cD galaxies

Figure 4.29 The cD NGC 4881 is located near the center of the Coma cluster and is surrounded by a swarm of much less luminous galaxies. [Figure courtesy of STScI]

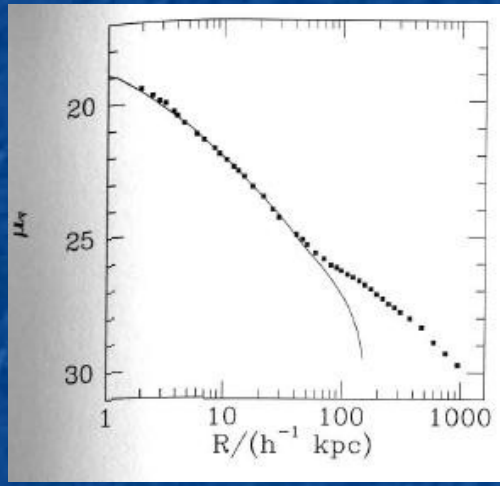

Figure 4.28 The surface-brightness profile of the cD galaxy that lies at the center of the cluster Abell 1413 (points). The line shows the $R^{1/4}$-law that best fits the inner points. [From data kindly provided by J. Schombert based on the work of Oemler (1976).]

Zdroj: Binney & Merrifield, Galactic Astronomy

Other profiles for ellipticals

- Hubble (or Hubble-Reynolds) profile (1913)

$$I(R) = \frac{I_0}{(1 + R/r_0)^2}$$

- modified Hubble profile: slide 32

- Sersic profile (1968)

$$I(R) = I_e 10^{\{-b_n[(R/R_e)^{1/n} - 1]\}}$$

Zdroj: Binney & Merrifield, Galactic Astronomy

2) Lenticular and spiral galaxies

bulge + exponential disk (Freeman, 1970)

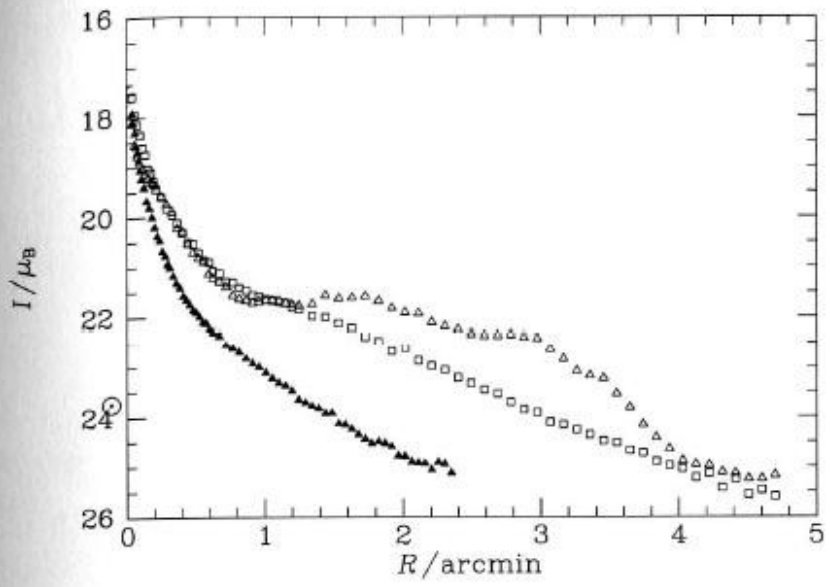

Figure 4.47 Blue surface brightness versus elliptical radius for three spiral galaxies: NGC 2841 (open squares); NGC 3898 (filled triangles); NGC 5194 (open triangles). The solar symbol ⊙ indicates the estimated surface brightness of the Milky Way near the Sun. The outer parts of two of the profiles are fairly straight in accord with equation (4.20). [From data published in Boroson (1981)]

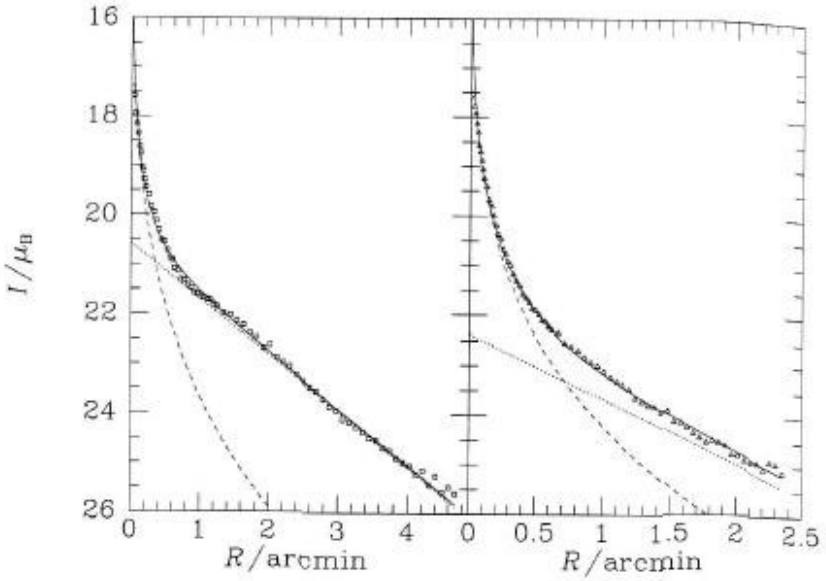

Figure 4.48 Fits to the surface-brightness profiles of NGC 2841 (left) and NGC 3898 (right). The dotted curves show the exponential fits to the disks and the dashed curves show the $R^{1/4}$ fits to the bulges; the full curves show the sums of these components. [From data published in Boroson (1981)]

Zdroj: Binney & Merrifield, Galactic Astronomy

From 2D to 3D: from surface brightness to volume density

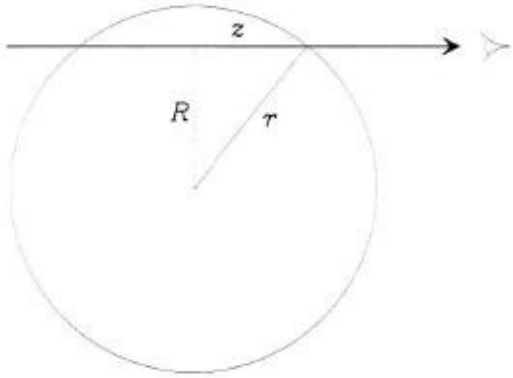

Figure 4.22 Projecting a spherical luminosity density along the line of sight.

$$I(R) = \int_{-\infty}^{\infty} \mathrm{d}z\, j(r) = 2\int_{R}^{\infty} \frac{j(r) r \mathrm{d}r}{\sqrt{r^2 - R^2}}.$$

$$j(r) = -\frac{1}{\pi}\int_{r}^{\infty} \frac{\mathrm{d}I}{\mathrm{d}R}\frac{\mathrm{d}R}{\sqrt{R^2 - r^2}}.$$

Zdroj: Binney & Merrifield, Galactic Astronomy

Example: modified Hubble profile

$$I(R) = \frac{I_0}{1 + (R/r_0)^2} \quad \leftrightarrow \quad j(r) = \frac{j_0}{[1 + (r/r_0)^2]^{3/2}},$$

$$L(R) \equiv 2\pi \int_0^R I(R') R' \, \mathrm{d}R' = \pi r_0^2 \ln \left[1 + (R/r_0)^2\right].$$

Zdroj: Binney & Merrifield, Galactic Astronomy

KAPITOLA II

Gravitační pole, Poissonova rovnice

Jednoduché modely galaxií:
dvojice potenciál-hustota, kruhová rychlost-rotační křivka, úniková rychlost

a) sféricky symetrické systémy
(logaritmický potenciál, Plummerova sféra, modifikovaný Hubbleův profil, homogenní sféra, singulární izotermální sféra

b) osově symetrické disky
Toomre-Kuzmin, Mestel, Miyamoto-Nagai, exponenciální disk

Gravitační pole, Poissonova rovnice

Dvojice potenciál-hustota: jednoduché modely galaxií

a) sféricky symetrické systémy
(Logaritmický potenciál, Plummerova sféra, modifikovaný Hubbleův profil, homogenní sféra, singulární izotermální sféra

b) osově symetrické disky
Toomre-Kuzmin, Mestel, Miyamoto-Nagai, exponenciální disk

Kruhová a úniková rychlost

Poisson equation, potential-density pairs

$$\nabla^2 \Phi = 4\pi G \rho.$$

$$\Phi(\mathbf{x}) = -G \int \frac{\rho(\mathbf{x}')}{|\mathbf{x}' - \mathbf{x}|} d^3\mathbf{x}',$$

$$\mathbf{F}(\mathbf{x}) = G \int \frac{\mathbf{x}' - \mathbf{x}}{|\mathbf{x}' - \mathbf{x}|^3} \rho(\mathbf{x}') d^3\mathbf{x}'.$$

Zdroj: Binney & Tremaine, Galactic Dynamics

Spherical systems

Newton's first theorem

A body that is inside a spherical shell of matter experiences no net gravitational force from that shell.

Newton's second theorem

The gravitational force on a body that lies outside a spherical shell of matter is the same as it would be if all the shell's matter were concentrated into a point at its center.

Zdroj: Binney & Tremaine, Galactic Dynamics

$$\Phi(r) = -4\pi G \left[\frac{1}{r} \int_0^r \rho(r') r'^2 dr' + \int_r^\infty \rho(r') r' dr' \right]$$

$$\mathbf{F}(r) = -\frac{d\Phi}{dr} \hat{\mathbf{e}}_r = -\frac{GM(r)}{r^2} \hat{\mathbf{e}}_r,$$

$$M(r) = 4\pi \int_0^r \rho(r') r'^2 dr'.$$

$$v_c^2 = r \frac{d\Phi}{dr} = r|\mathbf{F}| = \frac{GM(r)}{r}.$$

$$v_e(r) = \sqrt{2|\Phi(r)|}.$$

Zdroj: Binney & Tremaine, Galactic Dynamics

Homogeneous sphere, dynamical time

$$v_c = \sqrt{\frac{4\pi G\rho}{3}} r.$$

$$T = \frac{2\pi r}{v_c} = \sqrt{\frac{3\pi}{G\rho}},$$

$$\frac{d^2r}{dt^2} = -\frac{GM(r)}{r^2} = -\frac{4\pi G\rho}{3} r,$$

$$t_{\rm dyn} = \frac{T}{4} = \sqrt{\frac{3\pi}{16G\rho}}.$$

Zdroj: Binney & Tremaine, Galactic Dynamics

Simple potentials for galaxies

- Plummer potential (1911)

$$\Phi_P = -\frac{GM}{\sqrt{r^2 + b^2}}.$$

- Toomre-Kuzmin potential (1956, 1962)

$$\Phi_K(R,z) = -\frac{GM}{\sqrt{R^2 + (a + |z|)^2}}.$$

- Miyamoto-Nagai (1975) potential

$$\Phi_M(R,z) = -\frac{GM}{\sqrt{R^2 + (a + \sqrt{z^2 + b^2}\,)^2}}.$$

Zdroj: Binney & Tremaine, Galactic Dynamics

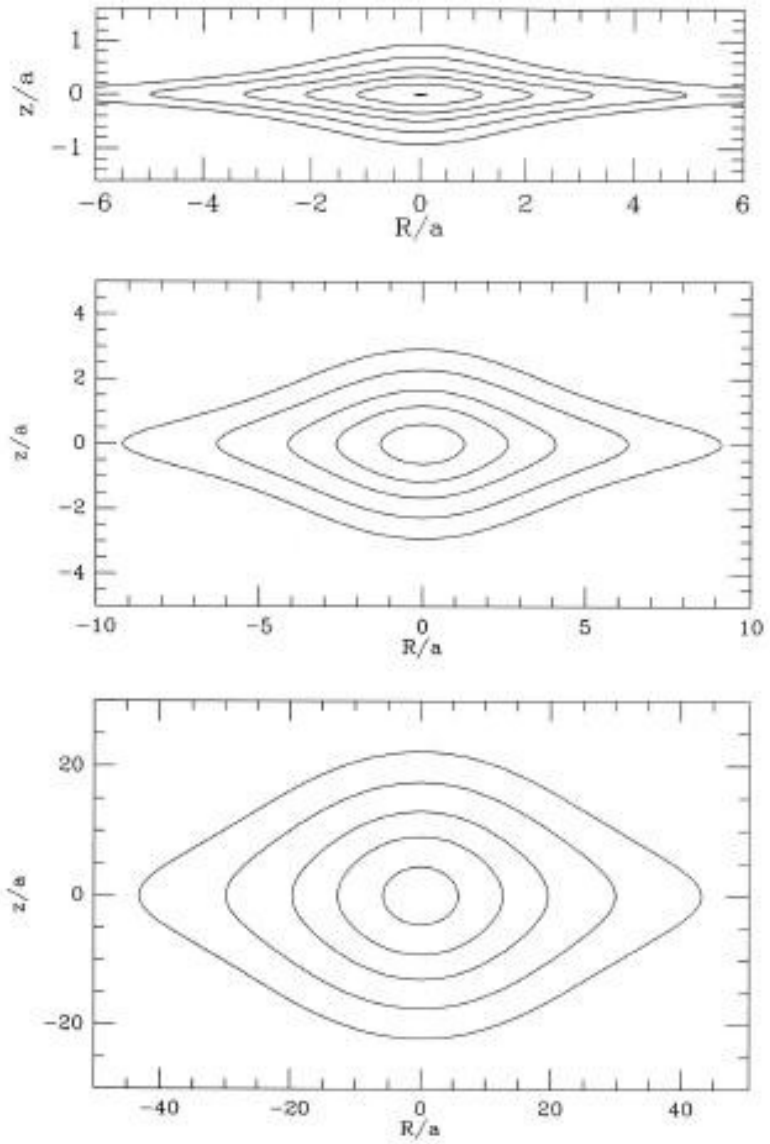

Figure 2-6. Contours of equal density in the (R, z) plane for the Miyamoto-Nagai density distribution (2-50b) when: $b/a = 0.2$ (top); $b/a = 1$ (middle); $b/a = 10$ (bottom). Contour levels are $f \times (1, 0.3, 0.1, 0.03, \ldots)$, where: $f = M/a^3$ (top); $f = 0.1M/a^3$ (middle); $f = 0.0001M/a^3$ (bottom).

Zdroj: Binney & Tremaine, Galactic Dynamics

Rotation curves of spiral galaxies

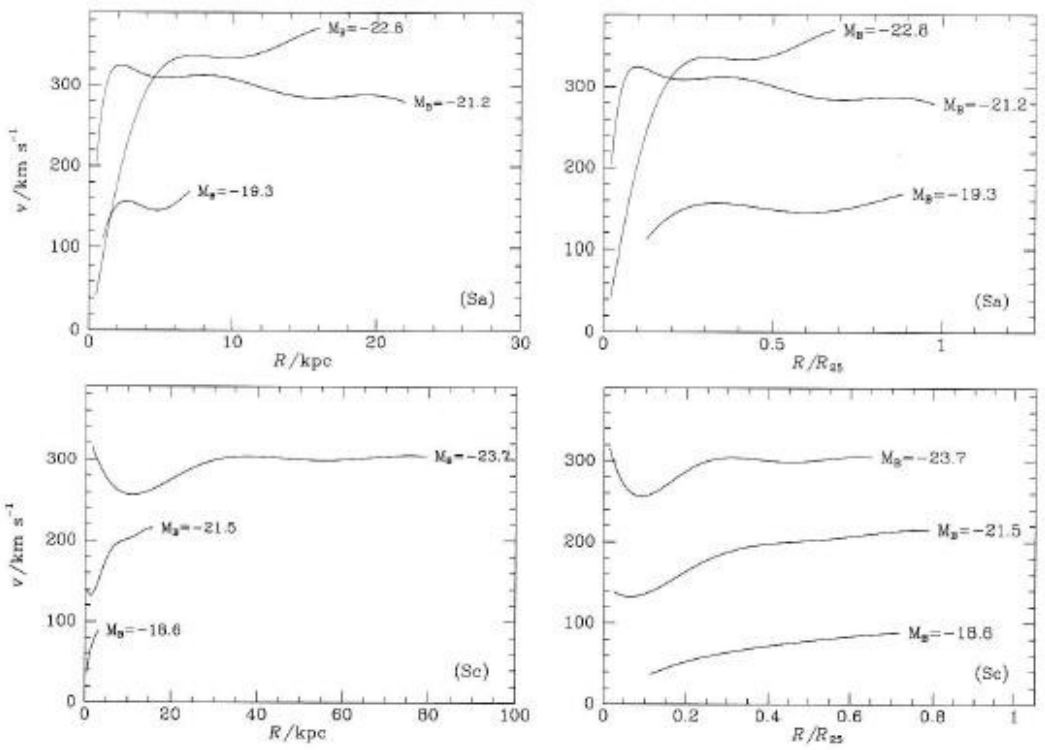

Figure 8.33 The upper panels show the rotation curves of three Sa galaxies of very different luminosities from the sample of Rubin *et al.* (1985) plotted both on the same linear scale (left) and rescaled by their optical radii, R_{25} (right). The lower panels show similar plots for three Sc galaxies from the sample of Burstein *et al.* (1982).

Zdroj: Binney & Tremaine, Galactic Dynamics

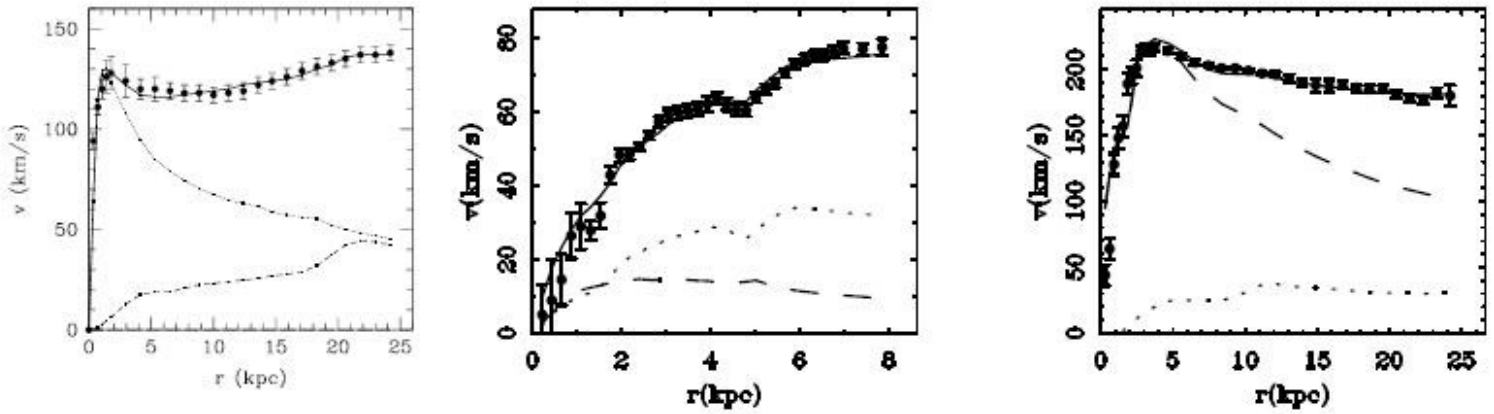

Fig. 2. The observed and MOND rotation curves (in solid lines) for NGC 3657 (left), NGC 1560 (cnter), and NGC 2903 (right). The first from Sanders (2006), the last two from Sanders and McGaugh (2002). Points are data, dashed and dotted lines for the last two galaxies are the Newtonian curves calculated for the stars and gas alone; the reverse for the first (they add in quadrature to give the full Newtonian curve).

Milgrom, 2009

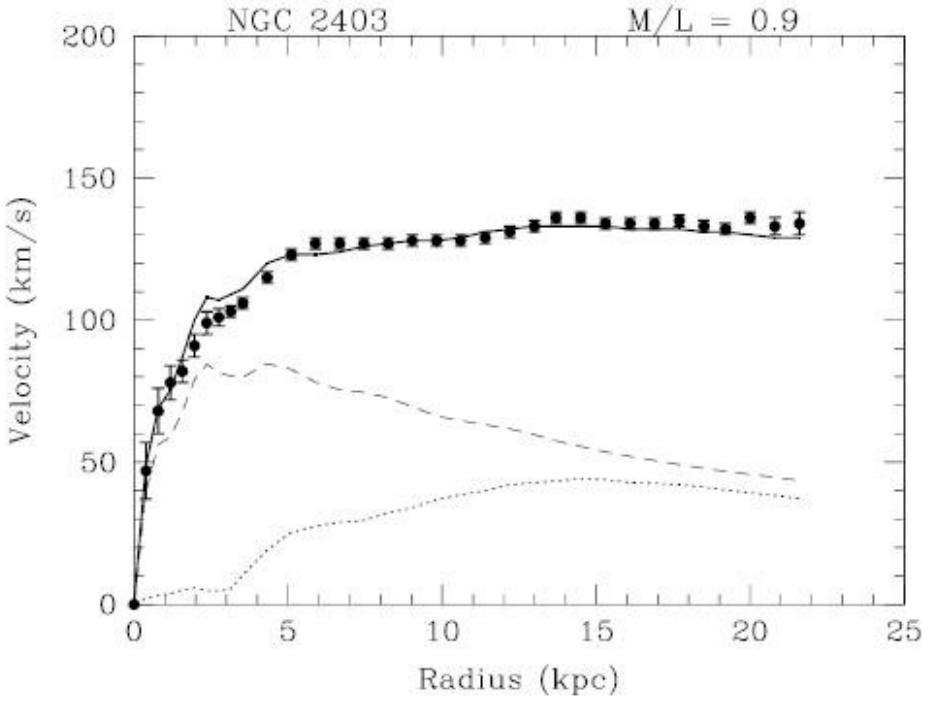

Figure 1: The points show the rotation curve of NGC 2403 as deduced from 21 cm line observations [6]. The dashed curve is the Newtonian rotation curve of the stellar component as deduced from the observed surface brightness distribution with M/L=0.9, and the dotted curve is the Newtonian rotation curve deduced from the observed HI surface density distribution. The solid curve is that calculated from Milgrom's formula. Here $a_0 = 10^{-8}$ cms^{-2}.

Sanders 2008

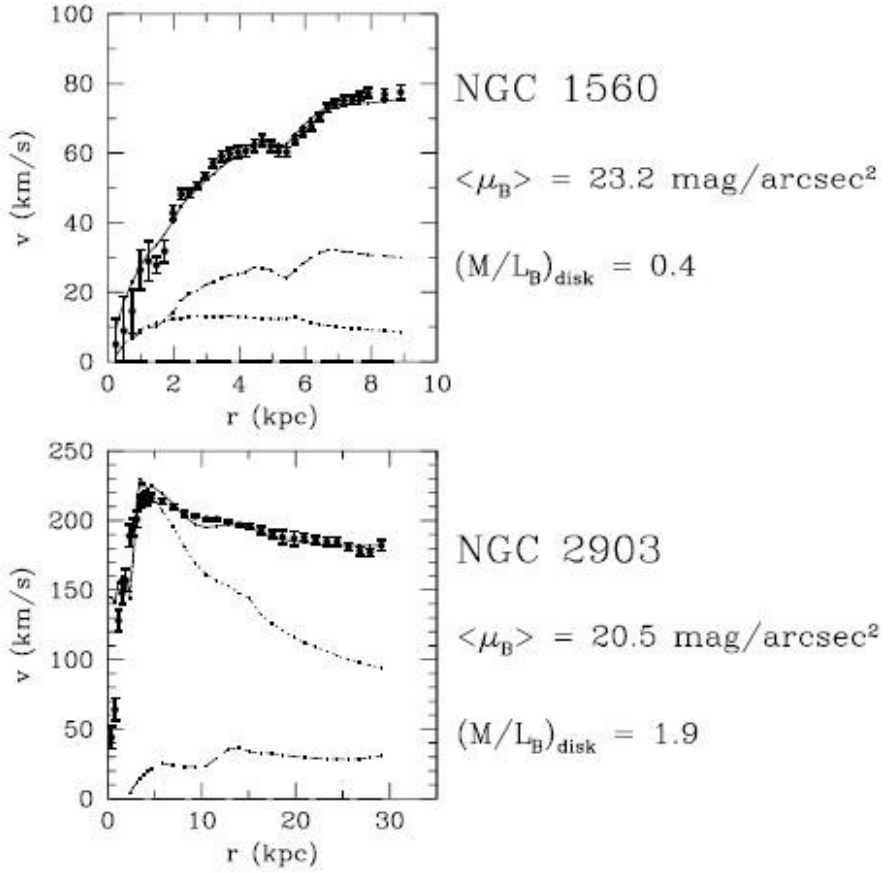

Figure 3: Observed rotation curves of a low surface brightness (Broeils [15])and a high surface brightness galaxy (Begeman [6]). Here the dotted curve is the Newtonian rotation curve of the stellar component and the dashed curve for the gas. The solid curve is the MOND rotation curve. The mean surface brightness and the implied mass-to-light ratios are indicated.

Sanders 2008

Logarithmic potential

$$\Phi_L = \tfrac{1}{2} v_0^2 \ln\left(R_c^2 + R^2 + \frac{z^2}{q_\Phi^2}\right) + \text{constant}$$

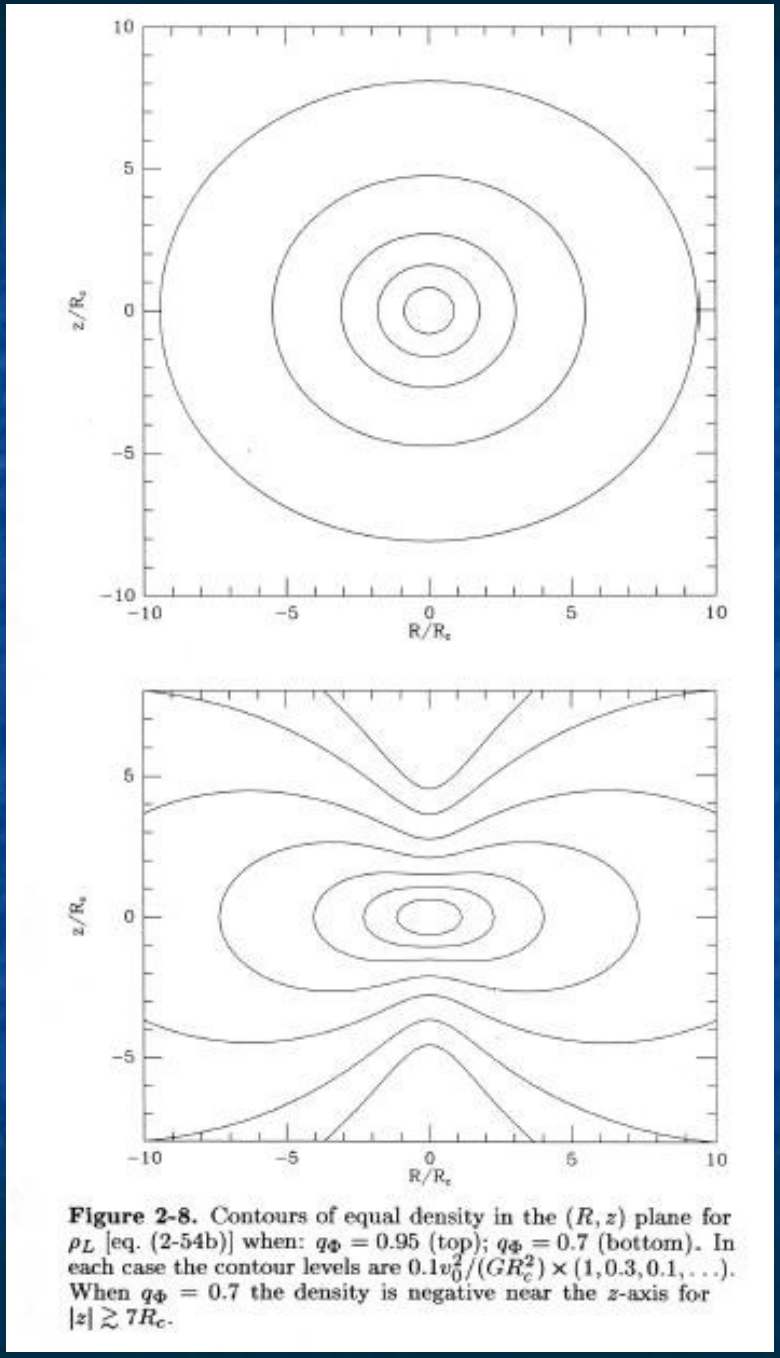

Figure 2-8. Contours of equal density in the (R, z) plane for ρ_L [eq. (2-54b)] when: $q_\Phi = 0.95$ (top); $q_\Phi = 0.7$ (bottom). In each case the contour levels are $0.1 v_0^2/(GR_c^2) \times (1, 0.3, 0.1, \ldots)$. When $q_\Phi = 0.7$ the density is negative near the z-axis for $|z| \gtrsim 7R_c$.

Zdroj: Binney & Tremaine, Galactic Dynamics

Epicyclic approximation for Keplerian orbits

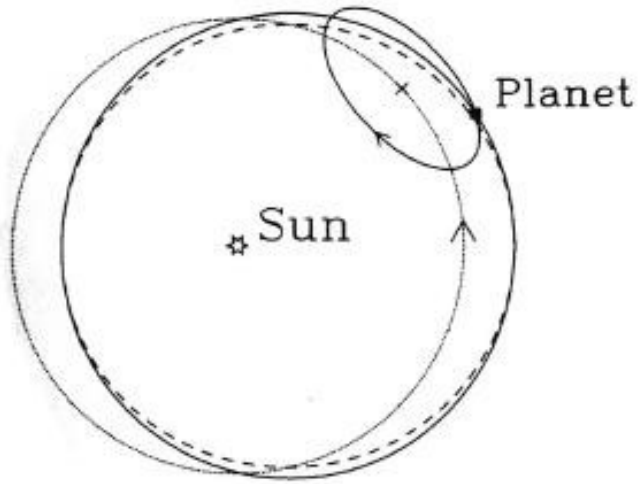

Figure 3-6. An elliptical Kepler orbit (dashed curve) is well approximated by the superposition of retrograde motion at angular frequency κ around a small ellipse with axis ratio $\frac{1}{2}$, and prograde motion of the ellipse's center at angular frequency Ω around a circle (dotted curve).

from Binney and Tremaine 1987

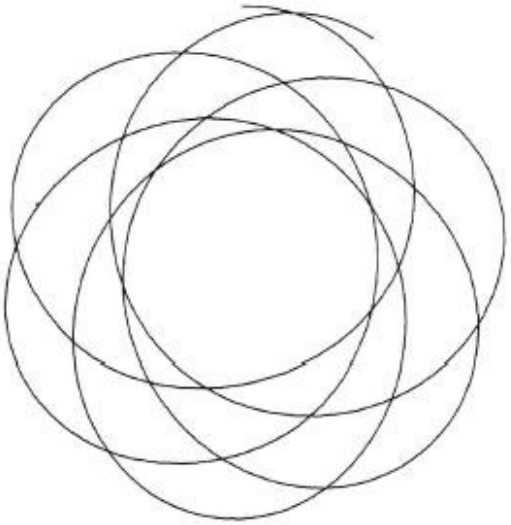

Figure 3-1. A typical orbit in a spherical potential forms a rosette.

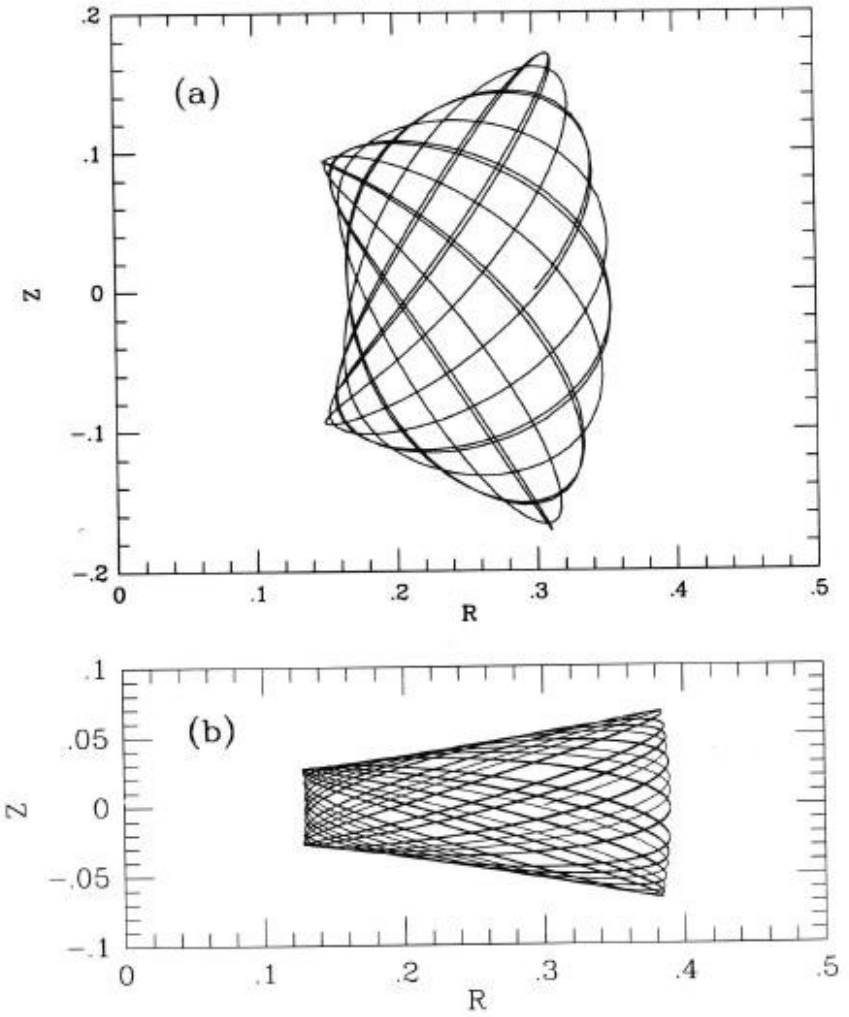

Figure 3-3. Two orbits in the potential of equation (3-50) with $q = 0.9$. Both orbits are at energy $E = -0.8$ and angular momentum $L_z = 0.2$, and we assume $v_0 = 1$.

Zdroj: Binney & Tremaine, Galactic Dynamics

Figure 3-7. Two orbits of a common energy, $E = -0.337$, in the potential Φ_L of equation (3-77) when $v_0 = 1$, $q = 0.9$ and $R_c = 0.14$: (a) a loop orbit; (b) a box orbit. The closed parent of the loop orbits is superposed on the orbit of (a).

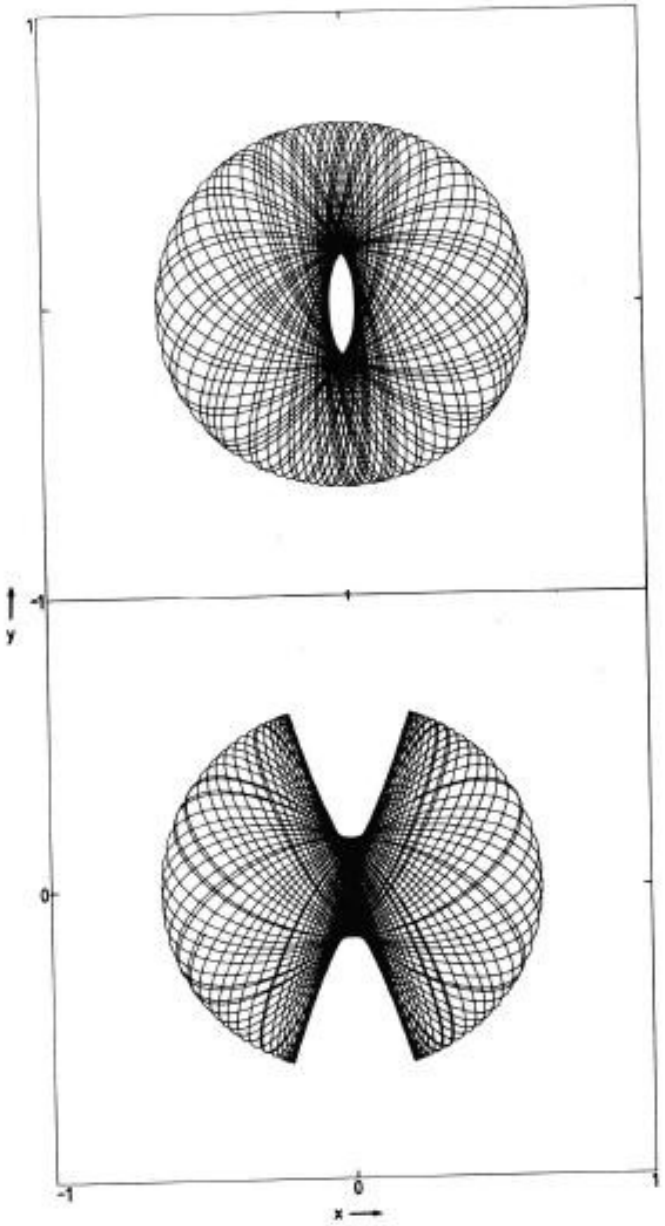

Figure 3-9. One of the most eccentric loop orbits and one of the least elongated box orbits in the potential $\Phi_L(q = 0.9, R_c = 0.14)$ at the energy of Figures 3-7 and 3-8.

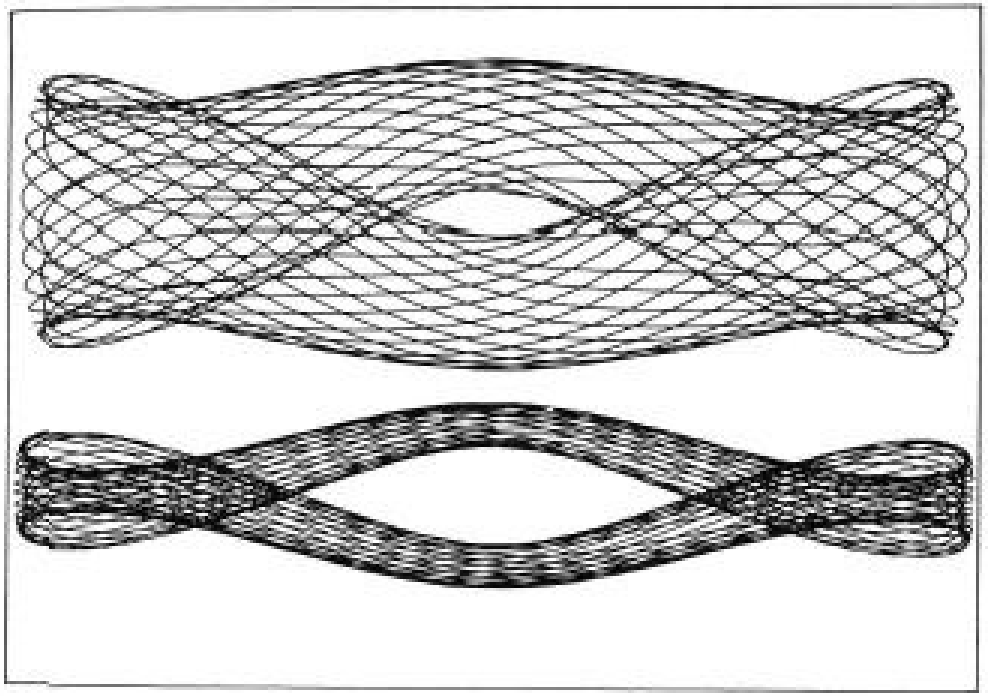

Figure 3-18. Two nonclosed orbits of a common energy in the rotating potential Φ_L.

Zdroj: Binney & Tremaine, Galactic Dynamics

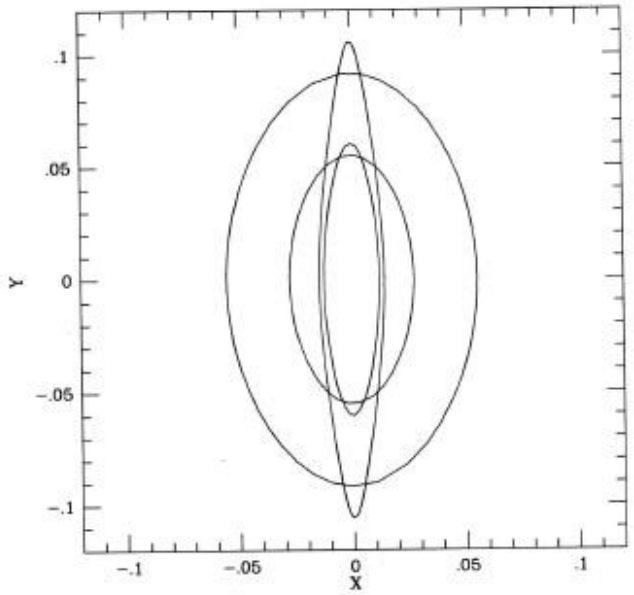

Figure 3-15. Closed orbits at two energies higher than those shown in 3-14. Just outside the potential's near-harmonic core there are at each energy two prograde closed orbits aligned parallel to the potential's short axis. One of these orbits (the less elongated) is stable, while the other is unstable.

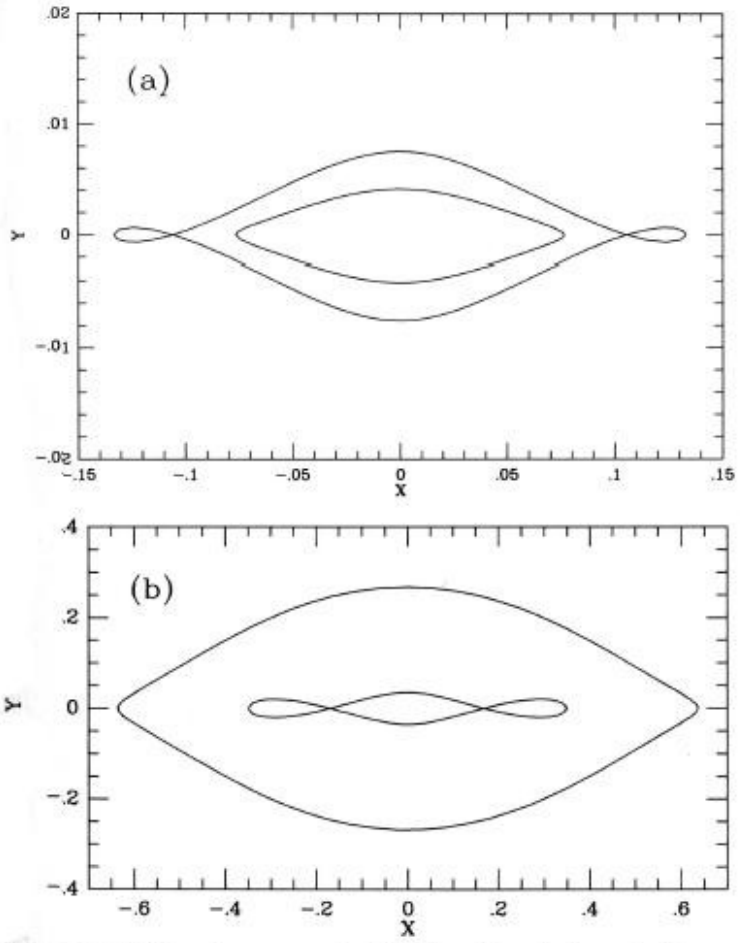

Figure 3-16. Near the energy at which the orbit pairs shown in Figure 3-15 appear, the closed long-axis orbits develop loops (a). At higher energies these expand, until the orbits open out into roughly elliptical figures (b). Notice that in (a) the x- and y-scales are different. In each diagram, two orbits at two different energies are shown.

Zdroj: Binney & Tremaine, Galactic Dynamics

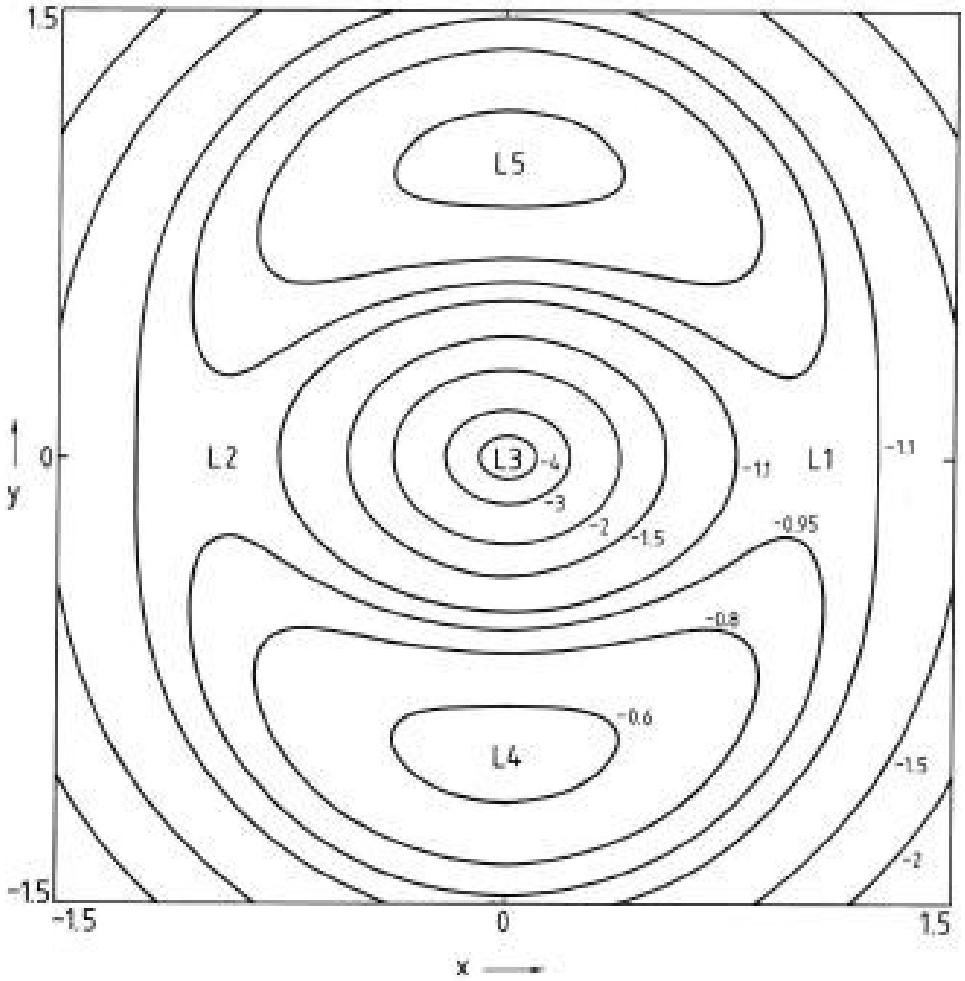

Figure 3-13. Contours of constant effective potential $\Phi_{\rm eff}$ when the potential is given by equation (3-77) with $v_0 = 1$, $q = 0.8$, $R_c = 0.1$, and $\Omega_b = 1$. The point marked L_3 is a minimum of $\Phi_{\rm eff}$, while those marked L_4 and L_5 are maxima. $\Phi_{\rm eff}$ has saddle points at L_1 and L_2.

Zdroj: Binney & Tremaine, Galactic Dynamics

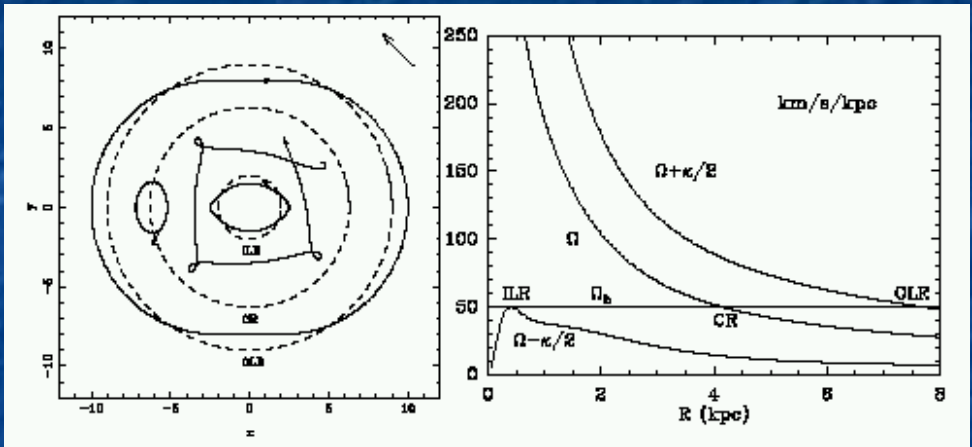

Buta & Combes 1996

Orbits in axisymmetric and barred potentials

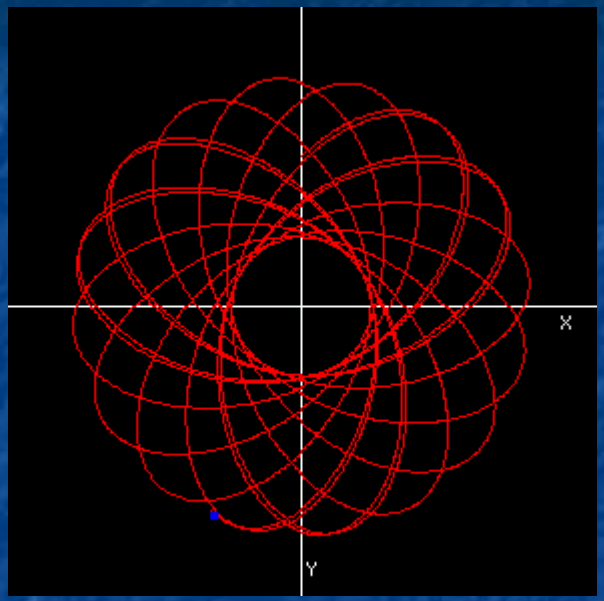

Stars

Gas

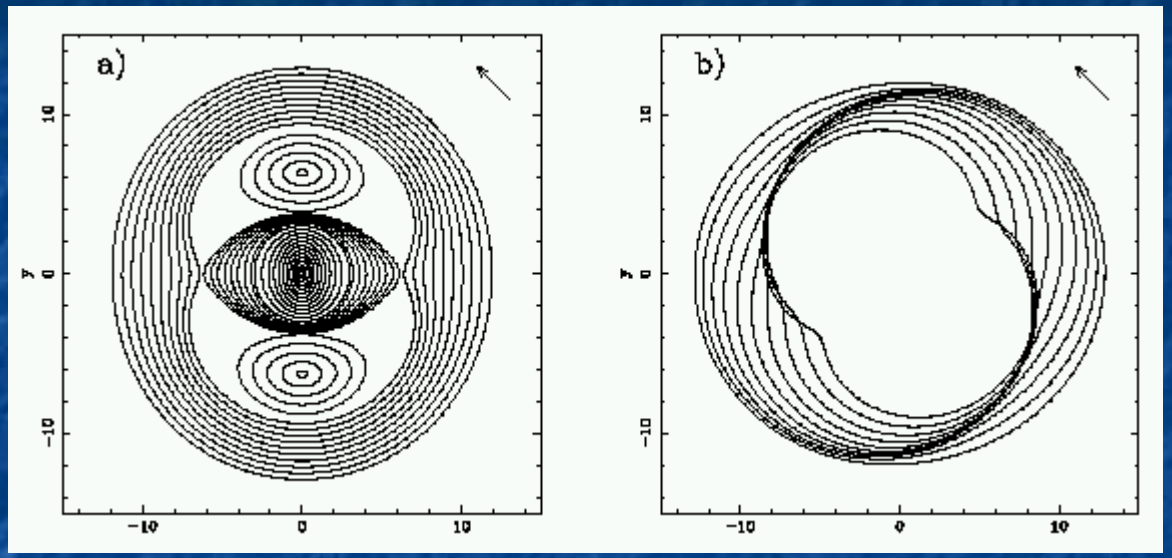

Gas

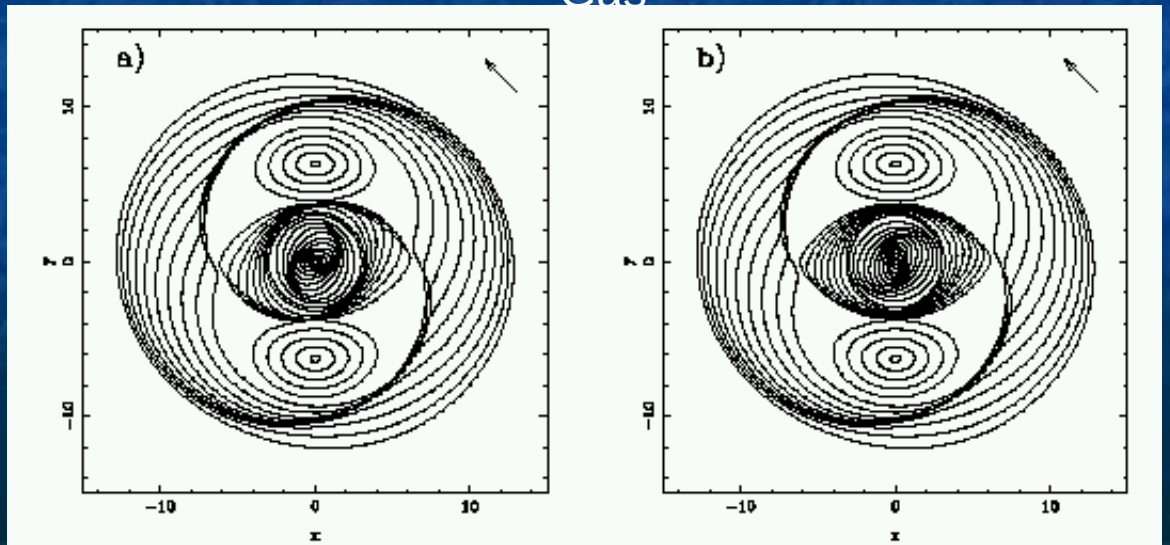

(from Combes 2003)

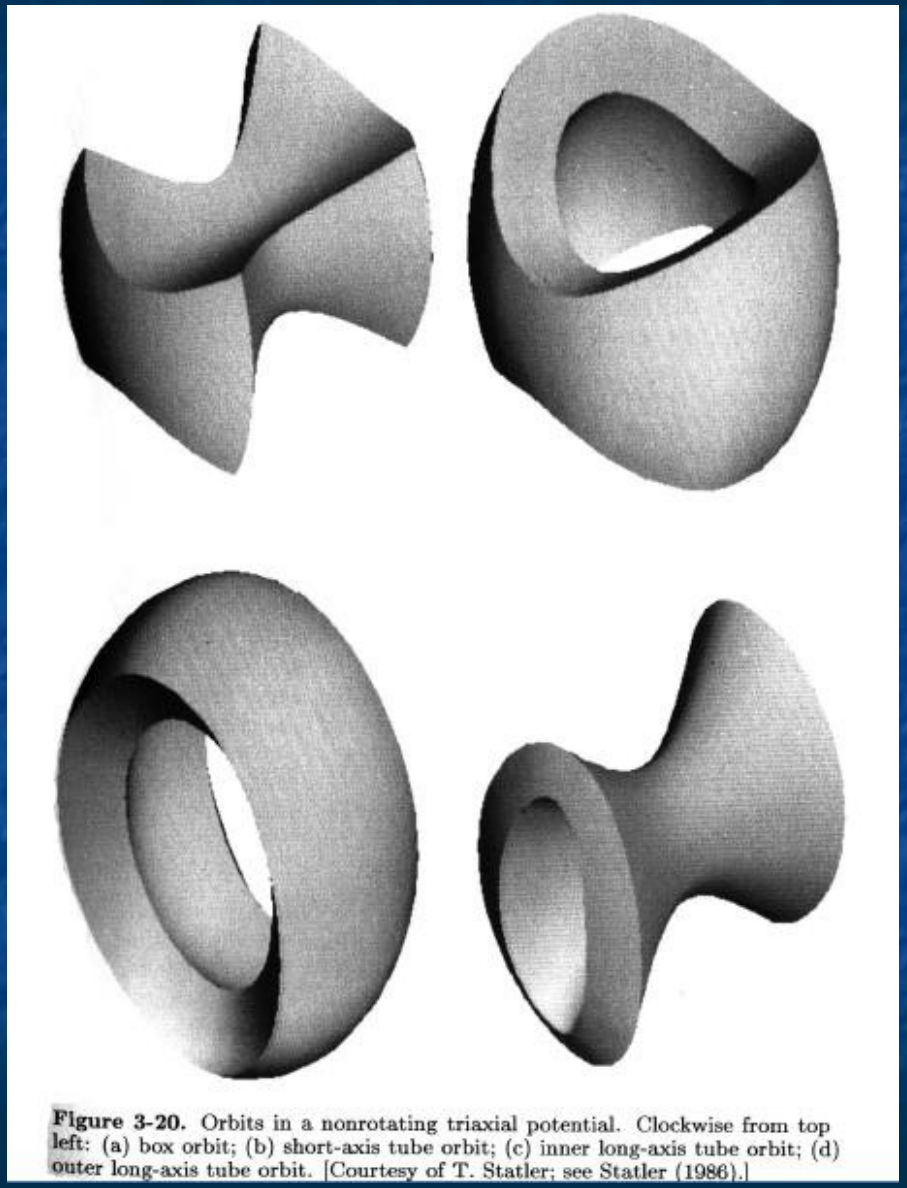

Figure 3-20. Orbits in a nonrotating triaxial potential. Clockwise from top left: (a) box orbit; (b) short-axis tube orbit; (c) inner long-axis tube orbit; (d) outer long-axis tube orbit. [Courtesy of T. Statler; see Statler (1986).]

Zdroj: Binney & Tremaine, Galactic Dynamics